Neural Network-based Synchronisation of Free-Floating Space Manipulator's Joint Motion and Mother Spacecraft's Attitude for Active Debris Removal

Shabadini Sampath
Dept. of Mechanical and Aerospace Engineering
University of Strathclyde
Glasgow, United Kingdom
shabadini.sampath@strath.ac.uk

Jinglang Feng
Dept. of Mechanical and Aerospace Engineering
University of Strathclyde
Glasgow, United Kingdom
jinglang.feng@strath.ac.uk

***Abstract*—A free-floating space manipulator attached to a spacecraft introduces challenges in simultaneously controlling the motion of the space manipulator and its mother spacecraft's attitude. This study aims to develop a neural network-based control approach to synchronously control the space manipulator motion and spacecraft attitude, improving the control performance in trajectory tracking, error reduction and eliminating uncertainties that arise from external disturbances, high-frequency noise, oscillations and imprecise knowledge of changes in the control system. Image-based Visual Servoing (IBVS) is used to provide inputs in terms of image features of the debris to the conventional controllers such as sliding mode control (SMC) and proportional-integral-derivative (PID). SMC is used to control the motion of the space manipulator. The unscented Kalman filter (UKF) provides the estimate of the spacecraft's attitude as an input to the PID controller to control the attitude. PID controller provides a feed-forward compensation to the SMC to counter spacecraft reactions to manipulator motion, while maintaining the attitude of the spacecraft. The neural network is introduced in the control strategy to enhance the performance of conventional controllers by dynamically optimising their gains and coefficients. This adaptability improves trajectory tracking accuracy, response to changes in the system and autonomy. The stability of this control approach is proven using the Lyapunov stability theorem, demonstrating a global asymptotic stability. The neural-network-based synchronous control approach is tested and validated by numerical simulations and comparative analysis in the MATLAB-Simulink environment. The results demonstrate an enhanced control performance in terms of accurate trajectory tracking, faster 100% convergence to zero error and more robustness to uncertainties. Outcomes highlight the potential of neural network-based control approaches in real-world applications that manage the free-floating space manipulators during uncooperative debris capture.**

***Index Terms*—Space manipulator, Sliding mode control, Proportional-integral-derivative control, Intelligent control, Active debris removal**

I. Introduction

The space sectors face a growing threat due to an increase in space debris that includes discarded spacecraft, rocket remnants and various man-made objects. Thus, in recent years, active debris removal (ADR) has emerged as a crucial strategy for mitigating space debris. This paper addresses this challenge by using a space manipulator attached to a spacecraft. In recent decades, the research on control of the spacecraft attitude has significantly grown due to its wide range of applications in various space missions such as earth imaging, spacecraft docking and rendezvous, satellite surveillance and multi-orbit tasks. During the on-orbit servicing (OOS), the manipulator's movements introduce perturbations to both translational and rotational motions of the spacecraft's platform. In a microgravity environment, due to the absence of weight, the spacecraft's platform reacts to torques and forces acting on it by the space manipulator. Therefore, the primary objective of the paper is to ensure the safe transfer of spacecraft to the proximity of the target object. This is achieved by precise control of the relative translation motion of the manipulator and synchronising the spacecraft's attitude. Achieving such a level of control is particularly challenging in the presence of uncertainties, such as external disturbances, high-frequency white noise and oscillations. The uncertainties make it difficult for controllers to precisely predict the spacecraft's behaviour and affect the performance efficiency and stability of the spacecraft system. Consequently, accurate attitude-tracking of spacecraft becomes a challenging problem. To overcome these challenges, this paper has incorporated neural network techniques to enhance the accuracy of synchronous control, automatically tune uncertainties, and augment the adaptability of the control system. The adaptive nature of the neural networks ensures a more responsive control strategy, significantly improving accuracy in trajectory tracking and stability in the spacecraft system.

Neural networks offer a unique capability to autonomously learn complex relationships from the data inherent in the system model that includes kinematics and dynamics of the space manipulator and spacecraft. Neural networks excel in modelling non-linear relationships and are well-suited for varying conditions where the inputs and outputs change over time. In a

International Strategic Partner, University of Strathclyde

study by [4], the research addressed the challenges with finite-time attitude tracking for a single spacecraft, highlighting the importance of precise control of the spacecraft. A few control algorithms have already been suggested for attitude control in papers [23], [25], [2] and [13]. Additionally, various effective nonlinear control techniques use neural networks for achieving accurate tracking control. In the study by [8], the research discusses the combined control of spacecraft with an unknown inertia matrix and external disturbances. Taking into account the recent studies that advocate for the integration of neural networks in attitude control, this research navigates through a comprehensive exploration of their application. Specifically, the paper explores how neural networks enhance the intelligence and robustness of conventional controllers, such as sliding mode controllers (SMC) and proportional-integral-derivative (PID) controllers. The adaptability of neural networks, adjusting controller parameters based on system dynamics and varying conditions, ensures a responsive control strategy, thereby significantly enhancing accuracy and stability.

The visual feedback extracted from the optical sensor is to realise the active motion control known as visual servoing. Image-based visual servoing (IBVS) is a control technique that utilises the visual information from the onboard cameras to control the attitude of the spacecraft. It computes the values for both the joint controller (SMC) and attitude controller (PID) directly based on the image features by eliminating the delay in the image interpretation and camera calibration errors. Using the image features, IBVS estimates the attitude (orientation) and then generates the control commands to align with the desired attitude. IBVS helps to improve the grasping accuracy during the capturing process of uncooperative debris. Additionally, the uncertainties that arise during the control performances are eliminated using neural networks. Sliding mode control (SMC) is a nonlinear control methodology designed to drive system states to a predefined "sliding surface" and maintain them on that surface. It excels in robustness against uncertainties and disturbances but may exhibit chattering, and rapid and high-frequency switching of the control signal. This characteristic has implications for practical implementations. In contrast, Proportional-Integral-Derivative (PID) control is a widely used feedback control strategy that adjusts the system output by calculating the proportional, integral, and derivative terms of the error. PID controllers are versatile and applicable to various systems but require careful tuning for optimal performance. Integrating neural networks with both SMC and PID controllers enhances adaptability and performance. Neural networks can learn system dynamics, facilitate adaptive tuning of controller parameters, and improve control responses under varying conditions, uncertainties, and disturbances. This integration contributes to the development of intelligent and robust control strategies that are crucial for addressing real-world challenges in diverse applications. An unscented Kalman filter (UKF) is used to estimate the attitude of the spacecraft with the input data obtained from the space manipulator, thereby facilitating precise spacecraft control and navigation. Furthermore, the neural network incorporated in the control framework enhances the capabilities of the UKF in tackling uncertainties and noise in measurements. The adaptability and capacity of the neural network to model complex relationships complement the UKF, contributing synergistically to enhancing the overall robustness and accuracy of the spacecraft orientation estimation process. This integrated approach represents a cutting-edge solution for addressing challenges associated with uncertainties in space manipulator systems.

II. Methodology

A spatial free-floating 3-DOF space manipulator attached to its mother spacecraft is schematically represented in Fig. 1. It consists of a spacecraft base (S), manipulator with 3 revolute joints, and end effector (E) to capture the target object (T). The target object is assumed to have a grapple fixture (G) for facilitating its capture. The dynamics of this system involve complex interactions between the manipulator, spacecraft, and target object. The inertial frame (I) provides a reference for understanding the overall motion and orientation of the system, enabling precise control and coordination of movements for tasks such as object manipulation and capture. The spacecraft body frame $[x_s, y_s, z_s]$, end effector's body frame $[x_e, y_e, z_e]$ and target object's body frame $[x_t, y_t, z_t]$ aligned with the inertia frame.

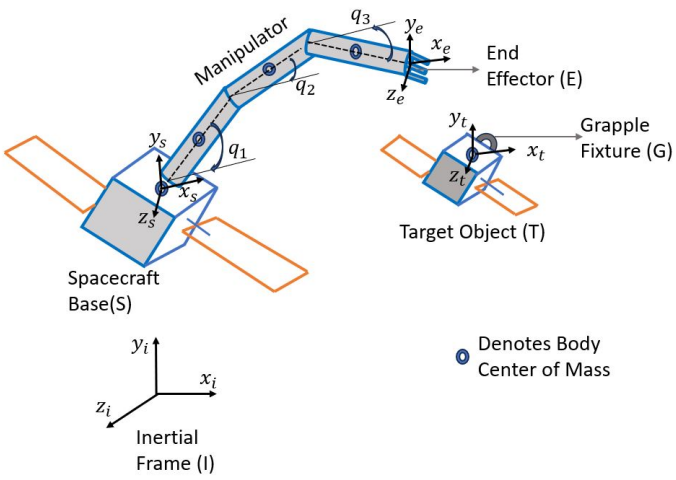

The methodology involves a novel neural network-based synchronized control approach, demonstrated in Fig. 1. The error between the desired image feature and the actual image feature serves as an input to the SMC alongside a predefined trajectory that steers the actual image feature towards the desired image feature. Simultaneously, the neural network processes input from the predefined trajectory. The SMC generates the required torque (τ_{SMC}), and this torque is combined with the neural network output (τ_{NN}) to govern the motion of the space manipulator by controlling the joint positions q. The combined torque is represented by (τ_m) in Fig. 1. Subsequently, the joint velocities $\dot{q}$are translated into spacecraft angular velocities $\dot{\theta}$, which serve as inputs to an Unscented Kalman Filter. The UKF estimates the actual state

of the spacecraft's attitude ($\hat{x}$). Using this estimated attitude, a Proportional-Integral-Derivative (PID) controller generates sufficient torque (τ_{PID}) to control the spacecraft's attitude. To achieve precision and accuracy in tracking the trajectory, the neural network again combined with the PID controller to control the attitude of the spacecraft. The resulting torque (τ_c) is applied as compensatory torque to the space manipulator, which is then applied to the space manipulator, ensuring that its motion aligns with the desired trajectory while maintaining synchronisation with the spacecraft's attitude. As demonstrated in Fig. 2, the output of the manipulator serves as an input to the spacecraft, enabling coordinated motion. This intricate control scheme aims to ensure precise control of both the manipulator's motion and the spacecraft's attitude, effectively addressing the challenges posed by the uncertainties during the uncooperative debris.

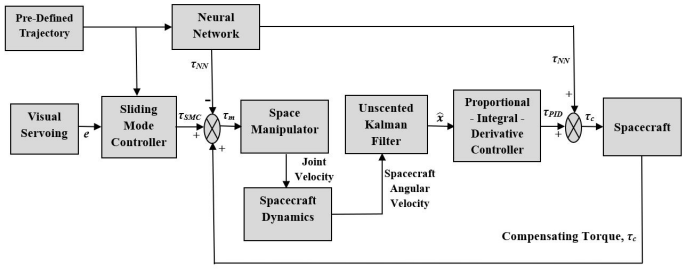

Fig. 1: Block diagram of Neural network-based synchronised control approach.

A. Image-Based Visual Servoing

Image-based visual servoing is a control technique that leverages visual information for precise control of the space manipulator. Unlike traditional control methods that solely rely on numerical data, visual servoing integrates real-time visual feedback to guide the motion of a space manipulator. The primary objective is extracting features by employing Harris Corner detection through the functions in MATLAB, yielding a set of corner points that highlight the desired image features [18]. These Harris corners are visualized on the extracted images to validate the accuracy of the detection process. These extracted features are used as input for conventional controllers. By having IBVS in the control loop, this control approach aims to improve the adaptability and responsiveness of the control system in uncooperative debris recognition.

$$e = I(m(r(t)),\ C) - I^*(t) \tag{1}$$

where e is the error between desired image features $I^*(t)$ and actual image features $I(m(r(t)),\ C$ is the camera's intrinsic parameters such as focal length, pixel aspect ratio, and lens distortion parameters. To effectively control the movement of the space manipulator, $I - I^*$ must be minimised, which is regulated by a sliding mode controller.

Taking the derivative of e with respect to time, the following equations are obtained:

$$\dot{e} = \frac{\partial I}{\partial m}\frac{\partial m}{\partial r}\frac{\partial r}{\partial t} + \frac{\partial I}{\partial C}\frac{\partial C}{\partial t} - \frac{dI^*}{dt} \tag{2}$$

The matrix Z and vector V_c is defined as follows:

$$Z = \begin{bmatrix}\frac{\partial I}{\partial m}\frac{\partial m}{\partial r} & \frac{\partial I}{\partial C}\end{bmatrix} \tag{3}$$

$$V_c = \begin{bmatrix}\frac{\partial r}{\partial t} \\ \frac{\partial C}{\partial t}\end{bmatrix} \tag{4}$$

$$\dot{e} = ZV_c - \dot{I}^* \tag{5}$$

where Z is the image matrix containing intrinsic parameters of the camera such as focal length, which is given as follows:

$$Z = \begin{bmatrix}\frac{-f}{d} & 0 & \frac{x}{d} & \frac{-xy}{f} & \frac{-f^2+x^2}{f} & y \\ 0 & \frac{-f}{d} & \frac{y}{d} & \frac{f^2+y^2}{f} & \frac{-xy}{f} & -x \\ \frac{-f}{d} & 0 & \frac{x}{d} & \frac{-xy}{f} & \frac{-f^2+x^2}{f} & y\end{bmatrix} \tag{6}$$

where f is the focal length of the camera, d is the depth, representing the distance from the camera to the object in focus, x and y represents the positions in the image plane. The matrix relates the spatial velocity of the camera V_c to the camera's or end effector's linear and angular velocities.

B. Sliding Mode Control

Image-based visual servoing (IBVS) commonly applies a proportional gain to minimise the image feature errors [7]. However, this method might lack the precision required for effectively capturing the target object. To address this limitation, sliding mode control is used in this research. SMC employs a predefined feature trajectory in the image plane as a guide to direct the actual image feature toward the desired features along this trajectory. By following this trajectory, SMC enhances the control precision and achieves the desired motion required for capturing the target object. The primary role of IBVS is to extract the relevant image features, while the SMC utilises these features to guide and optimise the motion control process. The tracking error in the SMC is defined as follows:

$$e = q - q_d \tag{7}$$

$$\dot{e} = \dot{q} - \dot{q}_d \tag{8}$$

$$\ddot{e} = \ddot{q} - \ddot{q}_d \tag{9}$$

where e is the error between the desired position and measured position, e, $\dot{e}$ and $\ddot{e}$ are supposed to be bounded, q_d, $\dot{q_d}$ and $\ddot{q_d}$ are the vectors of the desired position, velocity, and acceleration of the joint. The modified sliding surface s with visual servoing as input is given as follows:

$$s = I - I^* \tag{10}$$

$$\dot{s} = \dot{I} - \dot{I}^* \tag{11}$$

$$\dot{s} \equiv \dot{e} \equiv ZV_c - \dot{I}^* \tag{12}$$

The sliding surface is defined in equations (11) and (12), which will converge to 0 when the image features stay within the sliding surface during the approaching phase. The time derivative of the sliding surface is defined as follows [28]:

$$\dot{s} = \Lambda(\dot{q} - \dot{q_d}) - \ddot{q} + M^{-1}(q)[\tau - h(q,\dot{q}) - T_d - \alpha sin(s) - As] \tag{13}$$

where $M^{-1}(q)$ is the inverse inertia matrix, A is the robust term used in the neural network for tuning to achieve accurate trajectory tracking, T_d is the external disturbance and white noise in the control system, $h(q, \dot{q})$ is the centrifugal and Coriolis terms. By equating equation (12) and (13), the following equation is obtained;

$$V_c = \frac{M\Lambda\dot{e} - M\ddot{q} + (\tau - h(q,\dot{q})) - T_d - \alpha sin(s) - As + M\dot{I}}{MZ} \tag{14}$$

$$V_c = M^{-1}Z^{-1}[M\Lambda\dot{e} - M\ddot{q} + (\tau - h(q,\dot{q})) - T_d - \alpha sin(s) - As + M\dot{I}] \tag{15}$$

The control law for the SMC is obtained as follows:

$$V_c = Z^{-1}[\Lambda\dot{e} - \ddot{q} + M^{-1}(\tau - h(q,\dot{q})) - T_d - \alpha sin(s) - As + \dot{I}] \tag{16}$$

The joint velocity of the space manipulator is calculated using the velocity of the end effector ($\dot{q}$), which is given by the equation:

$$\dot{q} = M^{-1}V_c$$

C. Spacecraft Attitude Dynamics

The spacecraft's angular velocity ω can be related to the joint velocities $\dot{q}$ of the space manipulator using the transformation matrix. can be expressed as a function of the joint velocities of the space manipulator. $q = [q_1, q_2, ..., q_n]$ is the vector of joint positions and $\dot{q} = [\dot{q_1}, \dot{q_2}, ..., \dot{q_n}]$ is the vector of joint velocities of the space manipulator. The transformation matrix T that maps joint velocities to spacecraft angular velocities is rewritten as follows [22]:

$$\begin{bmatrix} \omega_x \\ \omega_y \\ \omega_z \end{bmatrix} = T(q,\dot{q}) \cdot \dot{q} \tag{17}$$

The coupling of spacecraft dynamics and space manipulator dynamics for coordinated control is considered a challenging task and the research is still ongoing. Equation (17) is rewritten in terms of the matrix as follows:

$$\begin{bmatrix} \omega_x \\ \omega_y \\ \omega_z \end{bmatrix} = \begin{bmatrix} 1 & \sin(\phi)\tan(\theta) & \cos(\phi)\tan(\theta) \\ 0 & \cos(\phi) & -\sin(\phi) \\ 0 & \sin(\phi)/\cos(\theta) & \cos(\phi)/\cos(\theta) \end{bmatrix} \begin{bmatrix} \dot{q}_1 \\ \dot{q}_2 \\ \dot{q}_3 \end{bmatrix} \tag{18}$$

Given the inertia tensor $\mathbf{I}$ as:

$$\mathbf{I} = \begin{bmatrix} 1 & \sin(\phi)\tan(\theta) & \cos(\phi)\tan(\theta) \\ 0 & \cos(\phi) & -\sin(\phi) \\ 0 & \sin(\phi)/\cos(\theta) & \cos(\phi)/\cos(\theta) \end{bmatrix} \tag{19}$$

D. Unscented Kalman Filter

The unscented Kalman filter is used to estimate the attitude of the spacecraft based on the manipulator's motion. The updated state estimate of the spacecraft is given as follows [3]:

$$x_{k|k} = x_{k|k-1} + K_k(z_k - z_{k|k-1}) = \hat{x} \tag{20}$$

where $x_{k|k-1}$ is the predicted state estimate at time k) based on the state at time $k-1$ and the system dynamics, z_k is the actual measurement related to the spacecraft's attitude at time k, $z_{k|k-1}$ is the predicted measurement at time $k|k-1$ based on the predicted state at the time $k|k-1$ and measurement function. The Kalman gain at time k is given as follows [3]:

$$K_k = P_{xz}(S^{-1}_{k|k-1}) \tag{21}$$

where P_{xz} is the cross-covariance matrix that relates the predicted state ($x_{k|k-1}$) with predicted measurement ($z_{k|k-1}$), $S^{-1}_{k|k-1}$ is the inverse of the predicted measurement covariance matrix that represents the uncertainty in the predicted measurement.

E. Proportional-Integral-Derivative Controller

The estimated state of the spacecraft is defined as follows:

$$\hat{x} = [\hat{\Theta_1}, \hat{\Theta_2}, \hat{\Theta_3}] \tag{22}$$

where $\hat{\Theta_1}$, $\hat{\Theta_2}$, and $\hat{\Theta_3}$ are the estimated Euler angles representing the spacecraft's attitude along x, y, and z axes, respectively. Consider the state covariance matrix of the estimated state as P, and it represents the uncertainty in the estimated state.

The PID controller uses the error between the desired attitude and the estimated attitude of the spacecraft to estimate the control torque τ. The error in estimated attitude is given by the following equation:

$$e_\Theta = \Theta_d - \hat{x} \tag{23}$$

where e_Θ is the attitude error of the spacecraft. The PID controller then calculates the control signal based on the attitude error e_Θ and the control gains K_p, K_i, and K_d for the proportional, integral, and derivative components, respectively:

$$u = K_p(e_\Theta) + K_d(\dot{e_\Theta}) + K_i(\int e_\Theta dt) \tag{24}$$

F. Neural Networks

The neural network architecture chosen for this research is shown in Fig. 2. The neural network consists of input layer with 2 neurons, hidden layer with 20 neurons and output layer with 2 neurons. The equations of the inputs, x_1 and x_2, and outputs of the neural network, τ_{NN}, with different weights $\hat{W}$ and W_i, in respective layers are derived in this section.

To address concerns about convergence and computational complexity, the proposed neural network approach incorporates a multi-layer architecture with adaptive weights. Initially, these weights adjust the sliding surface's slope, the gains associated with sliding mode control (SMC), and the control input, derived from error and its rate of change:

$$x_1 = [e_i, \dot{e}_i\ddot{e}_i]^T \tag{25}$$

The updated values of the gains will be derived in the cost function section. The first layer's output is expressed as:

$$y_i = \Lambda_i x_i \tag{26}$$

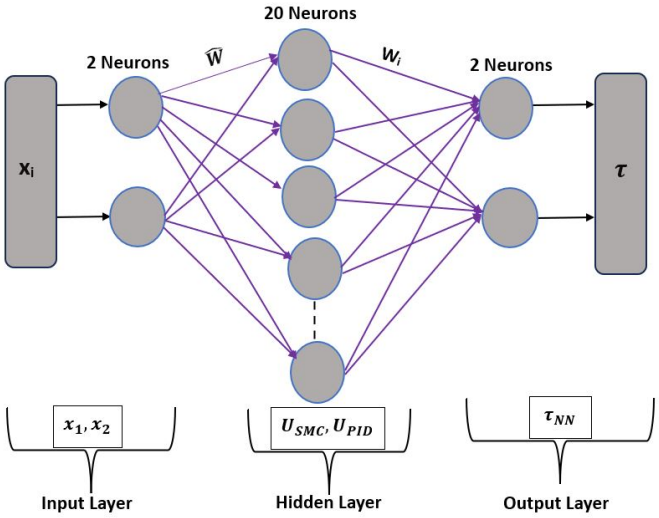

Fig. 2: Neural Network Architecture

where Λ represent the respective gain of e_i and $\dot{e}_i$. The modified sliding surface is computed as:

$$s_i = f_i(y_i) \tag{27}$$

where $f_i = (ZV_C - \dot{I})$ represents the activation function of the respective neuron in the neural network, where $\dot{I}$ is an unit matrix of 3*6 order for simplification in simulation purposes.

The hidden layer's input is formulated as:

$$K_{Np} = K_p + (\eta)(\beta)(e)(s_i) + \Gamma \tag{28}$$

where η is the positive constant and β represents the coefficients in the controller that are fine-tuned to achieve desired control performance by reducing the effects of sensor noise when used in conjunction with the Kalman filter. In this research, Γ is introduced representing an uncertainty that is challenging to predict precisely or model accurately. This uncertainty could arise from imprecise knowledge of system dynamics. Therefore, Γ is associated with uncertainties that the neural network aims to learn and compensate for, enhancing the system's robustness and adaptability. Γ is represented by a random number block generator to model uncertainties arising from imprecise knowledge.

$$K_{Nd} = K_d + (\eta)(\beta)(e)(\dot{e})(\sin(s_i)) \tag{29}$$

$$K_{Ni} = K_i + (\eta)(\beta)(e)(\dot{e})(\ddot{e})(s_i) \tag{30}$$

With K_p, K_i and K_d in the PID controller, the neural network adjusts these gains to help eliminate steady-state errors e and rate of error$\dot{e}$ providing stability to the controller. Also allows the control system to adapt to changing uncertainties.

$$x_2 = [s_{i1}, s_{i2}, K_{Np}, K_{Nd}]^T \tag{31}$$

With $s_{i1} = s_i$, $s_{i2} = \sin(s_i)$, while K_{Nd} and K_{Np} serve as offset signals compensating the control input signal.

The hidden layer's output for SMC is defined as:

$$\Lambda_{N1} = \Lambda_1 - \eta_{\Lambda_1}(e_i^2)(\frac{\Delta q_i}{\beta\tau_i})\left(-K_{pi} - K_{di}\frac{qe^{-2s_i}}{(1+e^{-2s_i})^2}\right) \tag{32}$$

$$\Lambda_{N2} = \Lambda_2 - (\eta_{\Lambda_2})(e_i^2\dot{e}_i\frac{\beta q_i}{\beta\tau_i})\left(-K_{pi} - K_{di}\frac{qe^{-2s_i}}{(1+e^{-2s_i})^2}\right) \tag{33}$$

$$\Lambda_N = \frac{\Lambda_{N1}}{\Lambda_{N2}} \tag{34}$$

$$U_1 = -\Lambda_N(s_{i1}) - \Lambda_N(K_{Np}) \tag{35}$$

$$U_2 = -\Lambda_N(s_{i2}) - \Lambda_N(K_{Nd}) \tag{36}$$

$$U_{SMC} = [U_1, U_2] \tag{37}$$

The hidden layer's output for PID is expressed as follows:

$$U_{PID} = \sum_{n=1}^{N} x_i\hat{W} \tag{38}$$

where $\hat{W}$ is the weight added in the hidden layer of the neural network and is given as follows:

$$\hat{W} = \alpha(K_p e + K_d\dot{e} + K_i\int e\,dt) + \Delta_{NN} \tag{39}$$

where α is the tuning parameter used in the neural network to determine the influence of neural network correction term Δ_{NN} relative to conventional gains of PID controller. Thereby, enhancing the control signal based on its learned knowledge of the control system. The overall neural network output is given as follows:

$$\tau_{NN} = (U_{SMC})(U_{PID})(W_i) \tag{40}$$

where W_i is the loss function used in training the neural network, which is given as follows [15]:

$$W_i = \frac{1}{2}(\theta_d - \hat{x})^2 \tag{41}$$

The objective is to minimise this loss function, leading to more accurate results.

III. Results and Discussion

In this section, the controllers outlined in equations (16), (25) and (41) are tested using MATLAB-Simulink environment to demonstrate the performance of the network-based control approach. The three reference trajectories of the Euler angles that represent the position and attitude of the space manipulator and spacecraft are defined as follows:

$$q_{1d} = \frac{55}{2} + \frac{55}{2}\sin\left(\frac{2\pi\cdot 10}{10} - \frac{\pi}{2}\right)$$

$$q_{2d} = \frac{85}{2} + \frac{85}{2}\sin\left(\frac{2\pi\cdot 10}{10} - \frac{\pi}{2}\right)$$

$$q_{3d} = \frac{105}{2} + \frac{105}{2}\sin\left(\frac{2\pi\cdot 10}{10} - \frac{\pi}{2}\right)$$

The following control parameters are fine-tuned using networks to obtain the desired control performance:

- Camera Parameters
  - $f = 150$
  - $d = 2$
  - $x = 75$
  - $y = 100$
- SMC
  - $\Lambda = \begin{bmatrix} 50 & 100 & 100 \\ 100 & 50 & 100 \\ 100 & 100 & 50 \end{bmatrix}$
  - $M^{-1} = \begin{bmatrix} 1 & 2 & 3 \\ 1 & 2 & 3 \\ 1 & 2 & 3 \end{bmatrix}$
  - $T_d = \begin{bmatrix} 0.05 \\ 0.1 \\ 0.15 \end{bmatrix}$
  - $\alpha = 0.01$
  - $s = \begin{bmatrix} 0.2 \\ 0.3 \\ 0.4 \end{bmatrix}$
  - $A = \begin{bmatrix} 1 & 1 & 1 \\ 1 & 1 & 1 \\ 1 & 1 & 1 \end{bmatrix}$
- PID
  - $K_p = 12.5$
  - $K_d = 15$
  - $K_i = 12.5$
  - $\Delta = 0.5$
  - $\eta = 0.1$
  - $\beta = 0.5$
  - $\Gamma = 0.1$

When tuning these parameters, it is important to make the controller responsive to changes, such as desired state changes (setpoint changes) and environmental changes, while being robust to the impact of noise. If the controllers become overly sensitive to external disturbances and noise, the controllers will respond to fluctuations that are not reflective of the actual state of the system, leading to instability. Therefore, these parameters are traded off to strike the right balance between responsiveness and robustness, and the neural network plays a pivotal role in achieving this balance. With these carefully adjusted parameters, the enhanced trajectory tracking performance is demonstrated in Fig. 3. Both the space manipulator and spacecraft accurately and precisely follow the desired trajectory.

The output of the controllers, neural network, SMC, and PID, in terms of torque, is plotted using MATLAB-Simulink environment, which is demonstrated in Fig. 4. It shows that the output of the controllers follows each other's trajectory closely.

The angular velocity of both the space manipulator and spacecraft is demonstrated in Fig. 5. The figure illustrates a good convergence rate and responsive behaviours achieved with the help of neural network-based controllers. This collaborative approach ensures accurate and dynamic tracking of desired trajectories.

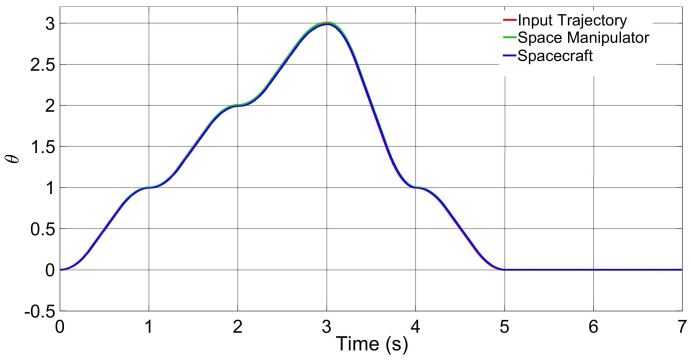

Fig. 3: Trajectory tracking performance of both space manipulator and spacecraft

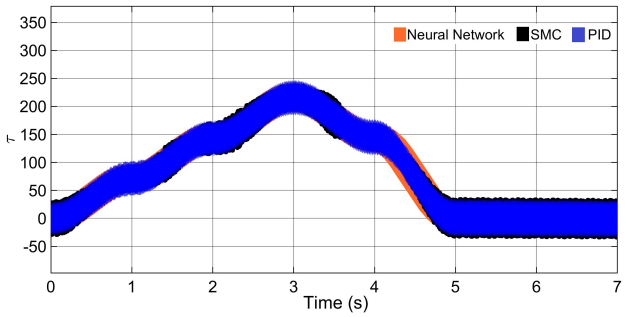

Fig. 4: Torque performance of the controllers

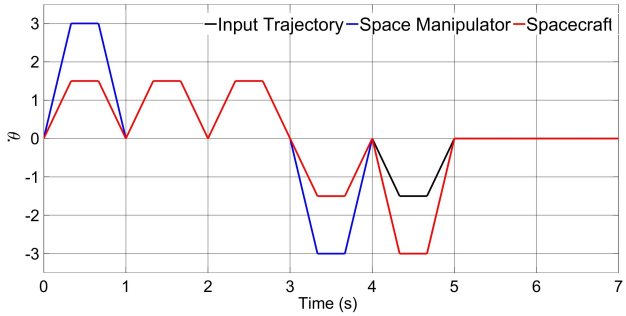

Fig. 5: Angular velocity performance of both space manipulator and spacecraft

Fig. 6 showcases the tracking errors for both the space manipulator and spacecraft. The convergence of these errors to zero is a positive indication that the controllers are successfully guiding the manipulator and spacecraft to closely follow the desired trajectories. This convergence is a key objective in the control design, as it signifies that the neural network-based controllers are capable of accurately steering the actual states to the desired states. This also indicates that the controllers are capable of managing the uncertainties, disturbances and any changes in the control system.

Additionally, the rate of error performance ($\dot{e}$) for both the space manipulator and spacecraft is demonstrated in Fig. 7.

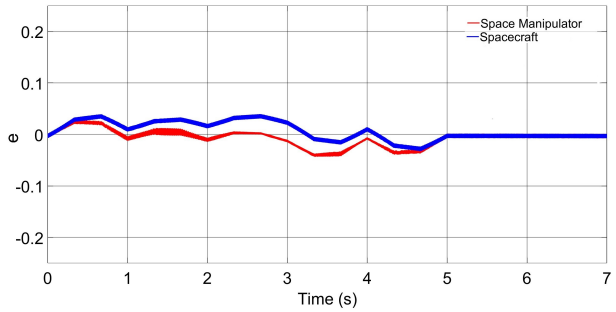

Fig. 6: Angular velocity performance of both space manipulator and spacecraft

This figure underscores the effectiveness of the neural network in enabling rapid adjustments and minimizing the rate of errors, contributing to the overall stability and precision of the control system.

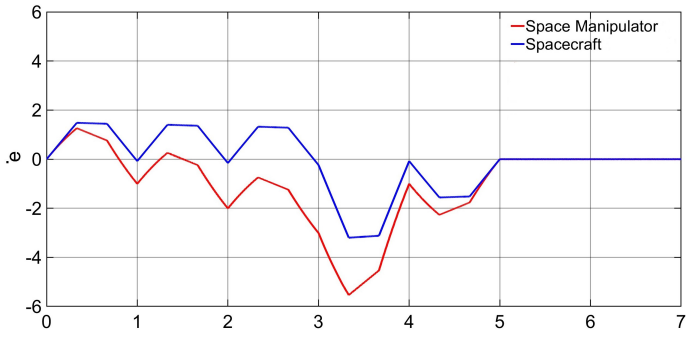

Fig. 7: The rate of error for both space manipulator and spacecraft

The stability of this control approach is also tested using the Lyapunov analysis theorem. The Lyapunov function (V) is a positive definite, denoted as $V > 0$, which means that the Lyapunov function has a positive value for all non-zero inputs, and it approaches zero only at the equilibrium point of the system. The primary purpose is to analyse the stability of the control system. Whereas, the time derivative of the Lyapunov function $\dot{V}$ is semidefinite and is denoted as $\dot{V} < 0$. The trajectory of the space manipulator and spacecraft must stay close to the sliding manifold. From Fig. 8, it is observed that ($\dot{V}$) is always negative, indicating that the control system has achieved global asymptotic stability. The Lyapunov function calculation is given as follows [10]:

$$\dot{V} \leq -s^T \alpha \sin(s) - s^T k s + s^T T_d \leq 0 \tag{42}$$

$$\implies s^T \alpha \sin(s) + s^T k s \geq s^T T_{\text{dbound}} \tag{43}$$

where $T_{\text{dbound}} = f(\dot{x}) = f_1 \dot{x} + f_2 \sin(\dot{x})$ and f_1 and f_2 are positive constant matrices.

IV. Comparison with Conventional Controllers

In the realm of neural networks, the assessment of the control performance is critical in measuring the efficiency of

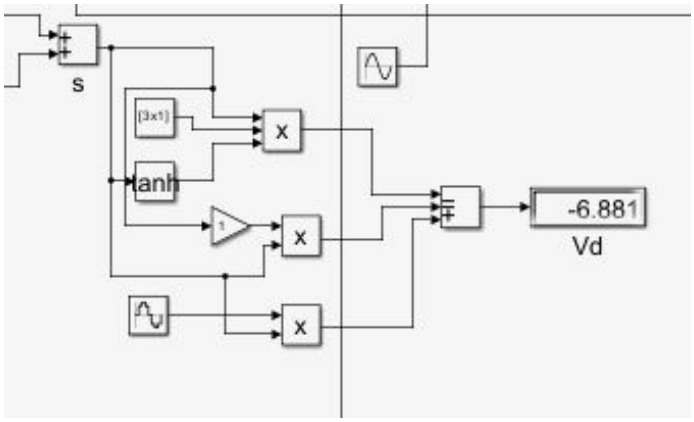

Fig. 8: The stability performance of neural-network-based synchronous control approach

the learning ability of the neural network. One prevalent metric employed for this purpose is Mean squared error (MSE) or loss function as shown in equation (43). The MSE provides a quantitative measure of the average squared between the predicted values generated by the neural network and the actual observed values from the input data.

The results obtained from the neural network show a very low value of 0.00029638 at Epoch 1000 as demonstrated in Fig. 9 and a very low is observed throughout the analyses [15]. This indicates that the neural network-based control approach provides accurate predictions and demonstrates a strong control performance during the training of the model in the network [17]. Low MSE also indicates that the neural network is robust to uncertainties.

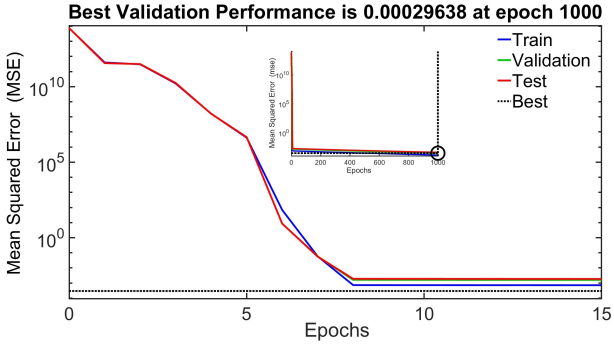

Fig. 9: Mean Squared Error performance vs Epoch

To test the efficiency of the proposed control approach, it is subjected to a comparative analysis against an alternative control scheme without neural network integration. This comparative study aims to highlight the distinctive advantages and improvements achieved through the incorporation of neural network-based control strategies. The comparison evaluation of trajectory tracking performance of both space manipulator and spacecraft is demonstrated in Fig. 10 and 4. Fig. 10 demonstrates that the space manipulator and spacecraft follow the trajectory but not closely, displaying less accuracy and

more pronounced discrepancies in the control system. The inherent uncertainties in the control system lead to deviation from the desired trajectory.

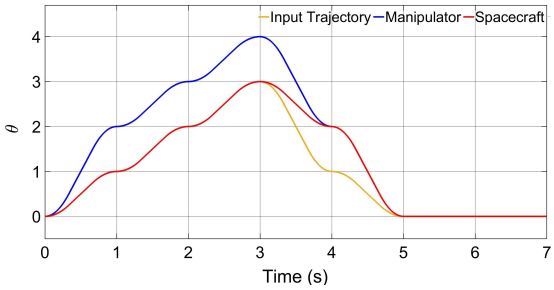

Fig. 10: Trajectory tracking performance of manipulator and spacecraft without neural network

In the presence of a neural network, both space manipulator and spacecraft exhibit a remarkable ability to closely follow the desired trajectory with high precision as demonstrated in Fig. 4. This is because of the capacity of neural networks to mitigate uncertainties and disturbances in the control system. This highlights the crucial role played by the neural network in enhancing control performance and trajectory tracking accuracy.

While the angular velocity trajectory performance, demonstrated in Fig. 11 and 5, exhibits a similar profile during both scenarios, the integration of a neural network in the control system significantly enhances the attitude controller's performance and accuracy. Fig. 11 demonstrates that there is a sudden change in control signals or disturbances in the control system, leading to sharp changes in system behaviour. Fine-tuning control parameters is done to ensure a smooth and gradual change in the control system response. The presence of the neural network enables the system to respond more effectively to dynamic changes and effectively attenuates the impact of noise and disturbances. This improvement is crucial for maintaining precise control and ensuring the system's adaptability to varying conditions.

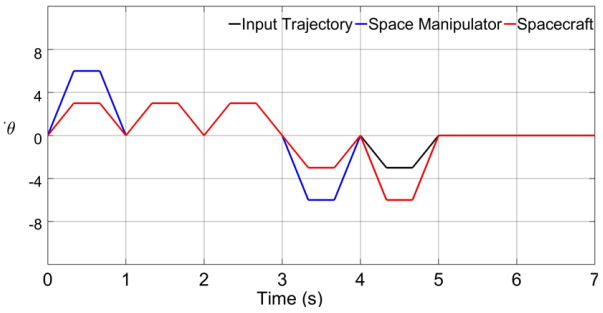

Fig. 11: The angular velocity performance of manipulator and spacecraft without neural network

In examining the error performance of both the space manipulator and spacecraft, the spacecraft experiences challenges in converging to zero error, requiring additional tuning to achieve convergence towards the end as demonstrated in Fig. 12.

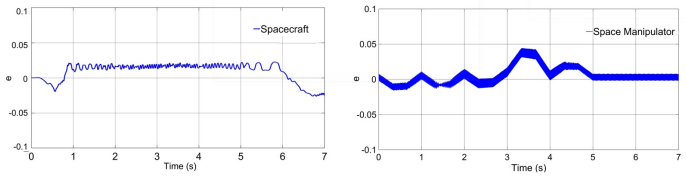

Fig. 12: The error performance of manipulator and spacecraft without neural network

Conversely, the neural network-based control approach significantly improves error reduction by attaining 100% convergence to zero seamlessly and efficiently. The consistent convergence to zero in the error plot in Fig. 6 indicates that the automatic tuning within the neural network is effective. This also suggests that the neural network is learning and optimizing control parameters in real time, leading to improvement in error reduction. Therefore, the neural-based control approach is more robust and has enhanced the control performance by addressing uncertainties and disturbances in the control system.

Analysing the rate of error performance, demonstrated in Fig. 13 and 7, reveals a clear enhancement in the neural network-based control approach. Fig. 13 demonstrates that the rate of error has a high magnitude, ranging between 10-15 units. However, the neural network-based approach in Fig. 7 demonstrates that the error has been significantly reduced between -4 to -6 units. The intriguing behaviour observed in the rate of error plot, where the plot transitions to the negative axis before converging, indicates that the neural network is not only compensating for the errors in the control system but also actively anticipating the errors and mitigating them. This negative value signifies a proactive corrective mechanism, showcasing the neural network's ability to enhance the control system's anticipation, and adaptability response to errors, ultimately guiding to a smoother convergence. This valuable trait of neural networks, especially in dynamic systems where real-time adjustments are crucial.

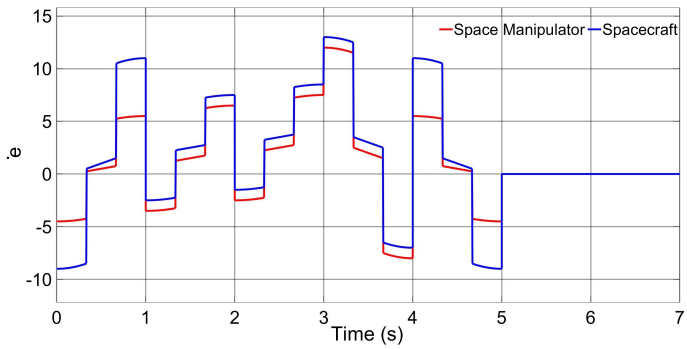

Fig. 13: The rate of error performance of manipulator and spacecraft without neural network

V. Conclusion

The integration of a neural network-based control approach in the synchronisation of free-floating space manipulator motion and mother's spacecraft attitude, within the framework of image-based visual servoing, demonstrates a spectrum of advantages, such as precision in trajectory tracking, adaptive response to uncertainties, dynamic disturbance, and noise rejection, improved system stability and mitigation of systematic errors that arise due to uncertainties in space manipulator and spacecraft. The control scheme leverages Image-based Visual Servoing (IBVS) for precise manipulation, while the unscented Kalman filter accurately estimates the spacecraft parameters, effectively mitigating camera noise. The fine-tuned control parameters, including robust terms in the sliding mode control, external disturbance compensation, coefficients and constant in the proportional-integral-derivative controller, and noise measurements in UKF, play pivotal roles in maintaining the trajectory accuracy and stability of the system. The neural network serves a crucial role in enabling the system to maintain a balance between responsiveness and robustness. The visual representation of error and rate of error plots underscores the adaptability nature of neural networks, resulting in 100% error reduction and convergence rate, and highly responsive control, significantly improving accuracy and stability. A comprehensive comparative analysis against the non-neural network counterpart validates the effectiveness of this intelligent control method, demonstrated through MATLAB-Simulink simulations. The synchronisation control of space manipulator motion with spacecraft attitude is a challenging task, especially in the presence of uncertainties and disturbances in the space environment. The neural network aids in overcoming these challenges, thereby improving the system's response during changes and noise. The direct comparison with a control approach devoid of neural network incorporation underscores the clear advantages of a neural network-based approach. Image-based visual servoing, coupled with the adaptability and learning capabilities of neural networks, enhances synchronisation, which is critical in space missions where precision and reliability are important. Challenges in fine-tuning are mitigated through the neural network's ability to adapt to changing conditions.

Acknowledgment

I would like to express my heartfelt gratitude to Professor Massimiliano Vasile, the Director of the Aerospace Centre of Excellence, for his unwavering support, guidance, and encouragement throughout this research study. I wish to express my sincere appreciation to the International Strategic Partner (ISP) of the University of Strathclyde for their generous funding that has played a crucial role in supporting my PhD studies. This financial support has allowed me to pursue my research goals and contribute to the body of knowledge in my field.

References

[1] Brannan, E. (2020). Debris Removal of Low Orbit Spacecraft Attitude Control System (ACS). [online] ResearchGate. Available at: http://doi.org/10.13140/RG.2.2.17824.40965.

[2] Chen, Z. and Huang, J. (2009). Attitude Tracking and Disturbance Rejection of Rigid Spacecraft by Adaptive Control. IEEE Transactions on Automatic Control, [online] 54(3), pp.600–605. doi:https://doi.org/10.1109/TAC.2008.2008350.

[3] Crassidis, J.L. and F. Landis Markley (2003). Unscented Filtering for Spacecraft Attitude Estimation. Journal of Guidance Control and Dynamics, 26(4), pp.536–542. doi:https://doi.org/10.2514/2.5102.

[4] Du, H., Li, S. and Qian, C. (2011). Finite-Time Attitude Tracking Control of Spacecraft With Application to Attitude Synchronization. IEEE Transactions on Automatic Control, 56(11), pp.2711–2717. doi:https://doi.org/10.1109/tac.2011.2159419.

[5] Felicetti, L. and Emami, M.R. (2018). Vision-Aided Attitude Control for Space Debris Detection. Journal of Guidance, Control, and Dynamics, 41(2), pp.573–575. doi:https://doi.org/10.2514/1.g002884.

[6] Fritz, M., Shoer, J., Singh, L., Henderson, T., McGee, J., Rose, R. and Ruf, C. (2015). Attitude determination and control system design for the CYGNSS microsatellite. 2015 IEEE Aerospace Conference. doi:https://doi.org/10.1109/aero.2015.7118962.

[7] Ghasemi, A. (2020). Enhanced Image-Based Visual Servoing Dealing with Uncertainties. core.ac.uk. [online] Available at: https://core.ac.uk/reader/335015330 [Accessed 23 Jan. 2024].

[8] Han, D., Dong, G., Huang, P. and Ma, Z. (2022). Capture and detumbling control for active debris removal by a dual-arm space robot. Chinese Journal of Aeronautics, [online] 35(9), pp.342–353. doi:https://doi.org/10.1016/j.cja.2021.10.008.

[9] Huo, X., Hu, Q. and Xiao, B. (2014). Finite-time fault tolerant attitude stabilization control for rigid spacecraft. ISA Transactions, [online] 53(2), pp.241–250. doi:https://doi.org/10.1016/j.isatra.2013.11.017.

[10] Hui Hu and Peng-Yung Woo (2006). Fuzzy supervisory sliding-mode and neural-network control for robotic manipulators. IEEE Transactions on Industrial Electronics, 53(3), pp.929–940. doi:https://doi.org/10.1109/tie.2006.874261.

[11] Kumar, A. (2020). An Overview of Visual Servoing for Robot Manipulators - Technical Articles. [online] control.com. Available at: https://control.com/technical-articles/an-overview-of-visual-servoing-for-robot-manipulators/.

[12] Lefferts, E.J., Markley, F.L. and Shuster, M.D. (1982). Kalman Filtering for Spacecraft Attitude Estimation. Journal of Guidance, Control, and Dynamics, 5(5), pp.417–429. doi:https://doi.org/10.2514/3.56190.

[13] Liu, E., Yang, Y. and Yan, Y. (2020). Spacecraft attitude tracking for space debris removal using adaptive fuzzy sliding mode control. Aerospace Science and Technology, 107, p.106310. doi:https://doi.org/10.1016/j.ast.2020.106310.

[14] Najafizadeh Sari, N., Jahanshahi, H. and Fakoor, M. (2019). Adaptive Fuzzy PID Control Strategy for Spacecraft Attitude Control. International Journal of Fuzzy Systems, 21(3), pp.769–781. doi:https://doi.org/10.1007/s40815-018-0576-2.

[15] Nielsen, M.A. (2015). Neural Networks and Deep Learning. Determination Press.

[16] Palmieri, G., Palpacelli, M., Battistelli, M. and Callegari, M. (2012). A Comparison between Position-Based and Image-Based Dynamic Visual Servoings in the Control of a Translating Parallel Manipulator. [online] Journal of Robotics. Available at: https://www.hindawi.com/journals/jr/2012/103954/.

[17] Pandit, M., Gaur, M.K., Prashant Singh Rana and Tiwari, A. (2022). Artificial Intelligence and Sustainable Computing. Springer Nature.

[18] Pomares, J. (2019). Visual Servoing in Robotics. Electronics, 8(11), p.1298. doi:https://doi.org/10.3390/electronics8111298.

[19] Ru, M., Zhan, Y., Cheng, B. and Zhang, Y. (2022). Capture Dynamics and Control of a Flexible Net for Space Debris Removal. Aerospace, 9(6), p.299. doi:https://doi.org/10.3390/aerospace9060299.

[20] Sakai, D., Yoshimura, Y., Hanada, T., Itaya, Y. and Fukushima, T. (2022). Contactless attitude control of an uncooperative satellite by laser ablation. Acta Astronautica, 196, pp.275–281. doi:https://doi.org/10.1016/j.actaastro.2022.04.024.

[21] Sampath, S., Feng, J., Marto, S.G. and Vasile, M. (2024). Image-based Synchronised Control of Spacecraft's Attitude and Space Manipulator's Motions for Capturing Uncooperative Targets. In: American Research Central. [online] AIAA SCITECH 2024 Forum. Reston: American Institute of Aeronautics and Astronautics, Inc. Available at: https://arc.aiaa.org/doi/epdf/10.2514/6.2024-2277 [Accessed 1BC].

[22] Singla, P., Duhan, M. and Saroha, S. (2022). 10 - Different normalization techniques as data preprocessing for one step ahead forecast-

ing of solar global horizontal irradiance. ScienceDirect. Available at: https://doi.org/10.1016/B978-0-323-90396-7.00004-3

[23] Srivastava, R., Sah, R. and Das, K. (2022). Attitude Determination and Control System for a LEO Debris Chaser Small Satellite. AIAA SCITECH 2022 Forum. doi:https://doi.org/10.2514/6.2022-0519

[24] Wilde, M., Kwok Choon, S., Grompone, A. and Romano, M. (2018). Equations of Motion of Free-Floating Spacecraft-Manipulator Systems: An Engineer's Tutorial. Frontiers in Robotics and AI, 5. doi:https://doi.org/10.3389/frobt.2018.00041.

[25] Xia, Y., Zhu, Z., Fu, M. and Wang, S. (2011). Attitude Tracking of Rigid Spacecraft With Bounded Disturbances. IEEE Transactions on Industrial Electronics, [online] 58(2), pp.647–659. doi:https://doi.org/10.1109/TIE.2010.2046611.

[26] Xiao, B., Yin, S. and Wu, L. (2017). A Structure Simple Controller for Satellite Attitude Tracking Maneuver. IEEE Transactions on Industrial Electronics, [online] 64(2), pp.1436–1446. doi:https://doi.org/10.1109/TIE.2016.2611576.

[27] Zhang, W., Li, F., Li, J. and Cheng, Q. (2023). Review of On-Orbit Robotic Arm Active Debris Capture Removal Methods. Aerospace, [online] 10(1), p.13. doi:https://doi.org/10.3390/aerospace10010013.

[28] Sampath, S. and Feng, J. (2024). Intelligent and Robust Control of Space Manipulator for Sustainable Removal of Space Debris. Acta astronautica, Volume 220, July 2024, Pages 108-117. doi:https://doi.org/10.1016/j.actaastro.2024.04.024.